

Interfacial Hydrothermal Assembly of Three-Dimensional Lamellar Reduced Graphene Oxide Aerogel Membranes for Water Self-Purification

Pengyu Zhuang, Zhongya Guo, Shuang Wang, Qi Zhang, Mingjian Zhang, Lili Fu,* Han Min, Bin Li, and Ke Zhang*



Cite This: *ACS Omega* 2021, 6, 30656–30665



Read Online

ACCESS |



Metrics & More

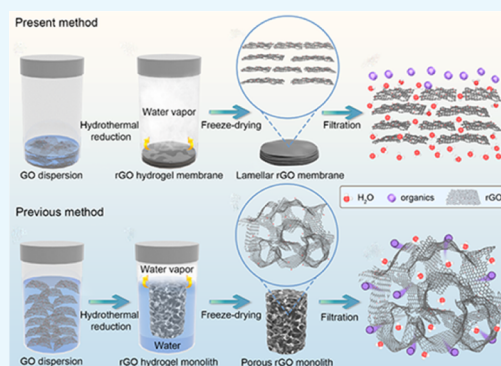


Article Recommendations



Supporting Information

ABSTRACT: Energy-saving membrane separation for water purification is increasingly desired, which requires appropriate nanofiltration membranes enabling to reject undesired solutes efficiently and allows high permeation of water. Herein, we report the fabrication of three-dimensional lamellar reduced graphene oxide (rGO) hydrogel membranes with a one-step, environment-friendly and water/vapor interfacial hydrothermal assembly process and the corresponding aerogel membranes by the freeze-drying method. The structures of the aerogel membranes can be tuned from lamellar to porously interconnected morphologies by controlling the volume of GO suspensions during the hydrothermal process. The rGO aerogel membrane was extremely flexible, which can be bent in liquid nitrogen and boiling water without any deformation, and highly stable in various solvents for at least 2 months. When used as nanofiltration membranes, the rGO aerogel membranes showed $\sim 100\%$ rejection of organic dyes and a moderate water flux (up to $53 \text{ L m}^{-2} \text{ h}^{-1}$) only under the gravity of organic dye aqueous solutions of a 30 cm height. This water self-purification property of our flexible and stable aerogel membranes without extra energy consumption provides a possibility to make cheap, portable water purification devices for utilization in emergency and home-used water purification systems in the areas with electricity unavailable or inconvenient.



1. INTRODUCTION

Energy-efficient membrane separations are increasingly demanded in a wide range of applications of desalination, water purification, chemical production, and petroleum refining.^{1–8} Graphene-based nanofiltration membranes with sub-nanometer- and nanometer-sized pores have attracted a great deal of interest in desalination^{4,9–11} and water purification^{12–14} due to their atomically thin two-dimensional nanosheets, which are desired to solve the trade-off dilemma between permeance and selectivity^{2,5,15–17} at a low cost of energy. Due to the one-atom thickness, flexibility, stability in chemical solvents, and strong mechanical properties, graphene is considered as an ideal barrier membrane^{18–21} by creating nanometer- and sub-nanometer-sized pores on the graphene membrane.^{22,23} However, it is a significant challenge to make uniform nanometer pores and transfer large-area graphene membranes to proper substrates without causing defects.^{23,24}

Graphene oxide (GO), as a derivative of graphene, can be synthesized in thousands of tons and dispersed well in water.^{18,20,25} Therefore, GO membranes can be easily fabricated in a large scale at a low cost. In addition, the sub-nanochannels between adjacent GO sheets can be tuned, which act as molecular sieving, being able to block all molecules and ions with hydrated diameters larger than the

sub-nanochannels,^{4,26,27} and GO membranes can be prepared with robust mechanical strength.²⁸ As a result, GO membranes have been universally studied in desalination, water purification, and molecular separation as nanofiltration membranes.^{4,14,18,26,27,29,30} However, the stability of GO nanofiltration membranes in water, especially in acid and basic aqueous media, is a significantly challenging problem,^{1,5,31} which restricts their practical application.

In order to improve the stability of GO membranes, reduced graphene oxide (rGO) membranes have been produced by chemically or thermally reducing GO membranes.^{18,24,27} After direct reduction, however, the rGO membrane showed a low water permeance^{18,27} and even became impermeable to water vapor when its thickness increased above micrometers²⁴ and became fragile. To improve water permeance of the rGO membrane and maintain its stability as well, people tried to

Received: August 17, 2021

Accepted: October 26, 2021

Published: November 3, 2021



Scheme 1. Schematic Fabrication of the rGO Hydrogel Membrane and Monolith via Water/Vapor Interfacial Hydrothermal and Bulk Hydrothermal Assembly Methods, Respectively, and the Corresponding Aerogel Membrane and Monolith by Freeze-Drying and Their Water Purifications

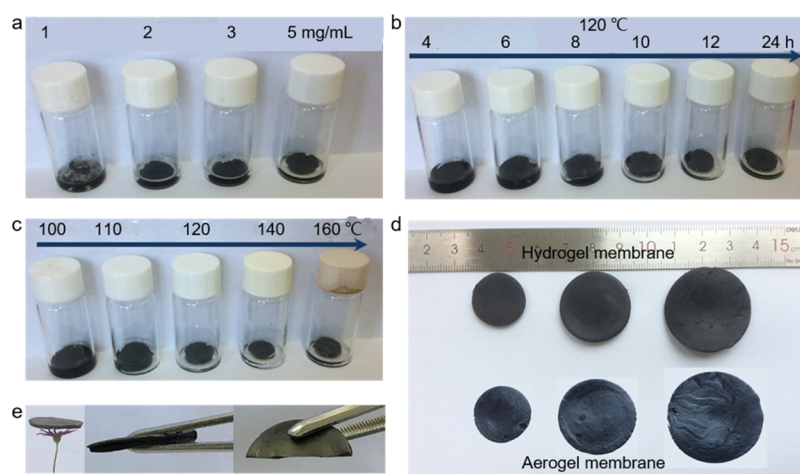
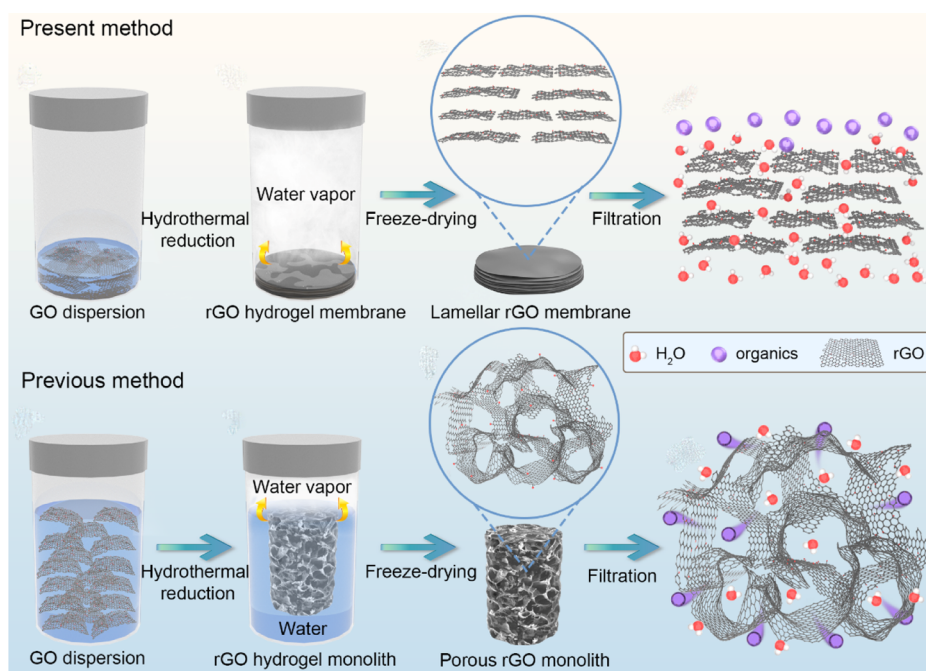


Figure 1. Fabrication of rGO hydrogel and aerogel membranes by interfacial hydrothermal assembly and freeze-drying methods. (a) Photographs of the products prepared with GO dispersions of different concentrations at 120 °C for 12 h. (b) Photographs of the products prepared with 5 mg mL⁻¹ GO dispersion at 120 °C for different times. (c) Photographs of the products prepared at different temperatures for 12 h with 5 mg mL⁻¹ GO dispersion. (d) Photographs of scalable rGO hydrogel and aerogel membranes prepared with 5 mg mL⁻¹ GO dispersion at 120 °C for 12 h. (e) Superlight and flexibility of rGO aerogel membranes.

mildly reduce GO nanosheets first without losing their dispersity in water at a short time and then prepared rGO membranes by vacuum filtration.^{6,13,31,32} Since, the rGO nanosheets are closely stacked together during the vacuum filtration process, forming dense two-dimensional lamellar membranes, these rGO nanofiltration membranes usually need to consume much energy in desalination and water purification.^{6,13,33} Therefore, the loose rGO nanofiltration membranes with both moderate water permeance and high selectivity and even without an extra energy cost need to be developed.

Hydrothermal reduction has been considered as an effective, facile, and environment-friendly self-assembly method in

synthesizing rGO hydrogels³³ and highly porous three-dimensional (3D) aerogels via a further freeze-drying process.^{35–37} rGO aerogels have been used in diverse applications of energy storage such as lithium batteries³⁸ and supercapacitors,³⁹ pollutant adsorption,^{40,41} and tissue engineering.^{36,42} However, the 3D lamellar rGO aerogel membranes have not been realized by combining the above methods and applied in water purification as nanofiltration membranes.

Here, we introduce a one-step water/vapor interfacial hydrothermal reduction method to assemble rGO hydrogel membranes under various conditions without adding any reducing reagents and their corresponding aerogel membranes

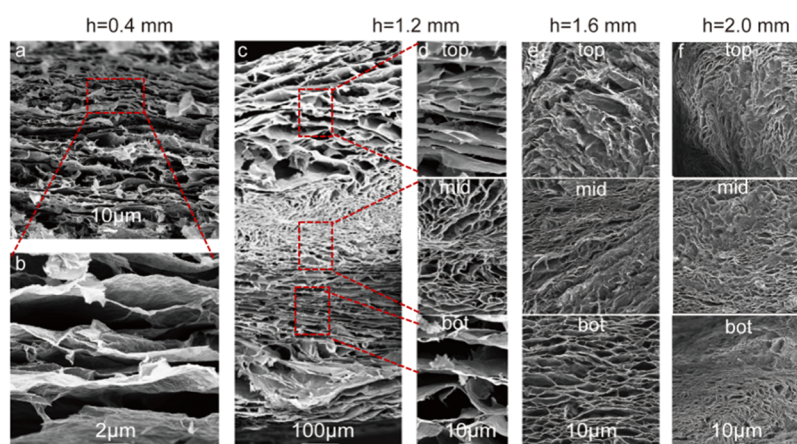


Figure 2. Cross-section morphologies of rGO aerogel membranes of different thicknesses. (a) Cross-section morphology of a 0.4 mm rGO aerogel membrane at a low resolution. (b) Cross-section morphology of the 0.4 mm rGO aerogel membrane. (c,d) Cross-section morphology of a 1.2 mm rGO aerogel membrane. (e) Cross-section morphology of a 1.6 mm rGO aerogel membrane. (f) Cross-section morphology of a 2.0 mm rGO aerogel membrane. Mid refers to middle, and bot refers to bottom.

via further freeze-drying. The structures of rGO aerogel membranes can be tuned from 3D lamellar to disordered interconnected morphologies by changing the volume per area (here called surface concentration) of GO dispersions. The rGO aerogel membranes were finally used as nanofiltration membranes for water purification only under the gravity of a 30 cm water column but still showed an excellent molecular selectivity of organic compounds and a moderate water permeance. The rGO nanofiltration membrane is especially suitable for making portable water purification devices and home-used water purification systems without costing extra power.

2. RESULTS AND DISCUSSION

2.1. Synthesis of rGO Hydrogel and Aerogel Membranes.

The GO used in this research was synthesized by the modified Hummers method^{43–45} with sheet sizes mainly in the range of 2–20 μm (Supporting Information, Figure S1). For the water/vapor interfacial hydrothermal reduction, only a small surface concentration (0.33–0.46 mL cm^{-2}) of GO suspension was used. It is unlike the previous bulk hydrothermal method,³⁴ in which much GO aqueous solution was used and occupied most volume of the container (Scheme 1). As a result, the assembly of rGO nanosheets could be proceeded at the interface between the little liquid water and vapor, even only at the vapor atmosphere. To visualize the assembly process of the GO aqueous solution, we first used transparent vials to synthesize rGO hydrogel membranes and then utilized Teflon containers of varied sizes to demonstrate the scalability of the rGO hydrogel and aerogel membranes (Figure 1). The interfacial hydrothermal assembly of rGO hydrogel membranes was first performed at 120 $^{\circ}\text{C}$ for 12 h by varying GO concentrations (Figure 1a). The GO nanosheets could be self-assembled into rGO hydrogel membranes when its concentration was higher than 1 mg mL^{-1} . The reaction times at a fixed GO concentration of 5 mg mL^{-1} were also tuned during the fabrication of rGO hydrogel membranes at 120 $^{\circ}\text{C}$ (Figure 1b). The height and size of the rGO hydrogel membrane started to decrease from 8 h but changed little since 12 h (Figure 1b). The GO sheets were only gelled but did not form an integrated membrane until 8 h. The rGO hydrogel membranes were also assembled at various temperatures

ranging from 100 to 160 $^{\circ}\text{C}$ for 12 h at a GO concentration of 5 mg mL^{-1} (Figure 1c). It can be seen that rGO hydrogels could be formed at all temperatures, and all water was kept in the hydrogel with no height change of the rGO hydrogel compared to the original height of GO solution at temperatures lower than 110 $^{\circ}\text{C}$. The integrated hydrogel membrane could not be generated until 110 $^{\circ}\text{C}$. With the temperature increased to 120 $^{\circ}\text{C}$, the rGO hydrogel became thinner and its size shrank a bit, and some free water fled from the hydrogel membrane. When the temperature increased further, the heights and sizes of rGO hydrogel membranes changed little, compared to the hydrogel membrane assembled at 120 $^{\circ}\text{C}$. Therefore, the rGO aerogel membranes for water purification were all prepared at 120 $^{\circ}\text{C}$ for 12 h at 5 mg mL^{-1} of GO. For water purification, nanofiltration membranes should be large enough and highly flexible for facile operation. Herein, the rGO hydrogel membranes were scaled up by changing the sizes of Teflon-line containers, and their corresponding aerogel membranes were produced by freeze-drying them (Figure 1d). Therefore, it is believed that the rGO aerogel membrane with a large size could be fabricated with proper containers. Furthermore, the rGO aerogel membrane has a superlight weight with a density of 17.5 mg cm^{-3} (Figure 1e). The aerogel membrane is extremely flexible, which can be folded (Figure 1e) and bent at an extremely low temperature such as in liquid nitrogen with a temperature of -196°C (Supporting Information, Video S1) or a high temperature of $\sim 100^{\circ}\text{C}$ in boiling water (Supporting Information, Video S2). After that, the aerogel membrane could still keep its integrity. Therefore, our rGO aerogel membrane has great potential for a nanofiltration membrane with a large size and flexibility for making portable water purification devices and home-used water purification systems.

2.2. Structure Characterization of rGO Hydrogel and Aerogel Membranes.

The lamellar structure of rGO membranes with suitable sub-nanochannels between the adjacent rGO sheets plays a key role in rejecting the solutes larger than the sub-nanochannels.¹⁸ However, the rGO nanofiltration membranes used in water purification are mostly prepared by vacuum-filtrating the slightly pre-reduced GO sheets, forming dense ultrathin lamellar membranes,^{6,31,33} which consume extra energy in practical applications. Herein,

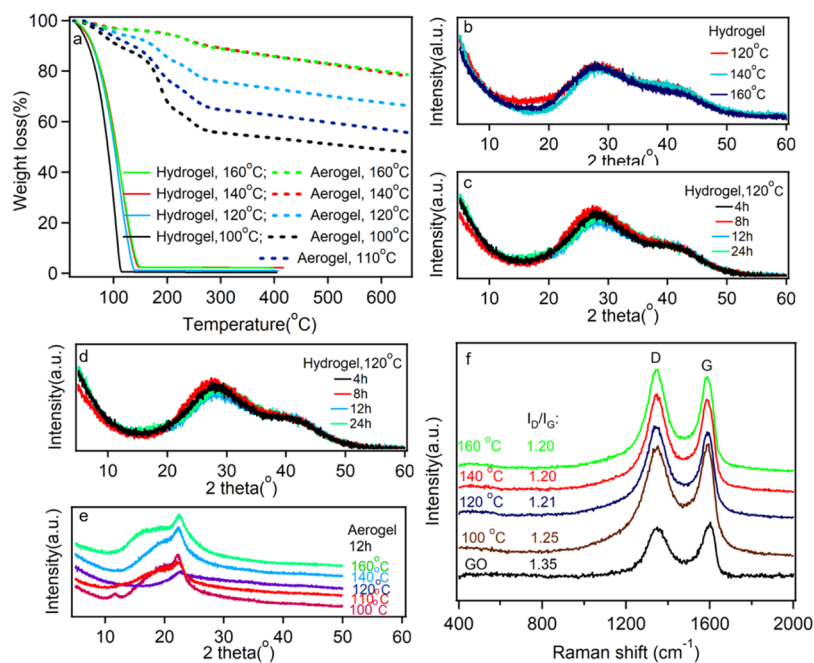


Figure 3. Characterizations of rGO aerogel membranes. (a) TGA data of rGO hydrogels and aerogel membranes prepared at different temperatures. (b–e) XRD data of rGO hydrogel and aerogel membranes prepared at different temperatures and different times at 120 °C. (f) Raman spectra of GO membranes and rGO aerogel membranes prepared at different temperatures for 12 h.

the rGO aerogel membrane prepared by the water/vapor interfacial hydrothermal reduction also shows a lamellar structure; however, the laminates are loosely stacked and cross-linked by the small laminate pieces (Figure 2a,b). In addition, the laminate consists of several thinner laminates, and there are also spaces between the thinner laminates.⁴⁶ For the membrane, a GO surface concentration of 0.33 mL cm⁻² was used. The rGO aerogel membranes prepared at different temperatures have similar structures, although the spaces between the laminates decreased with temperature (Supporting Information, Figure S2a,b,d,e,g,h). Besides, there are no visible pores on the aerogel membrane surfaces at the detected limit resolution of scanning electron microscopy (SEM), although the corrugations and wrinkles are generated on surfaces and become more obvious with the increase of temperature (Supporting Information, Figure S2c,f,i). This structure is absolutely different from the highly porous aerogel produced with the previous bulk hydrothermal method by Xu et al.,³⁴ which generated interconnected microporous pores.⁴⁷

The cross-section structural evolution of rGO aerogel membranes with thickness is studied. Different thicknesses of rGO aerogel membranes were generated by varying the GO surface concentration under the same conditions (120 °C, 12 h). When the thickness of the rGO aerogel membrane was ~0.4 mm, uniform laminates were produced (Figure 2a, Supporting Information, Figure S2d,e). When the thickness increased to 1.2 mm, the lamellar structures were formed at the top and bottom sections of the aerogel membrane, while the laminates were less ordered in the middle section of the membrane and interconnected pores were formed (Figure 2c,d). When the thickness increased to ~1.6 mm, no flat lamellar structures were formed. The top and middle parts of the membrane became disordered, although the bottom section maintained a parallel order to a certain extent, but were closely connected with each other, forming 3D pores (Figure 2e, Supporting Information, Figure S3). When the

thickness increased above 2.0 mm, the cross-section became completely disordered (Figure 2f, Supporting Information, Figure S4), in which the laminates were cross-linked with each other, creating pores of several micrometers similar to the 3D highly porous aerogel.³⁴ As can be seen, the structure of the hydrogel is sensitive to the GO surface concentration. When less volume of GO was used, it means that less water has smaller affection on the self-assembled process of rGO hydrogels because water evaporated and less water was left at the bottom. Besides, when a smaller volume GO was used, the thickness of the hydrogel membrane was thinner and the water vapor was able to escape from the bulk to outside of the hydrogel more easily, causing less influence on the self-assembly of the rGO hydrogel. Another reason for the lamellar structure formation is that the GO sheets preferred to be aligned parallel as nematic phase crystals.⁴⁵ When water has less effects on the self-assembly of the rGO hydrogel, the parallel rGO laminates are generated.

The water content of rGO hydrogels and the thermal stability of the rGO hydrogels and aerogel membranes prepared at different temperatures were studied by thermogravimetric analysis (TGA) (Figure 3a). The water content in hydrogels ranged from ~99.4 to ~97.6%, which decreased gradually with temperature up to 140 °C. After that, the water content changed little. The onset temperature of rGO hydrogels shows a similar trend to water content, which is a bit higher than the hydrothermal temperature, except for the hydrogel prepared at 160 °C. While the onset temperature of rGO decomposition starts at around 160 °C for each aerogel membrane. The main decomposition temperature of functional groups starts at ~160 °C and ends at ~270 °C, showing high temperature stability.

The interlayer spacings of adjacent rGO sheets in laminates of the rGO hydrogels and aerogel membranes were detected by X-ray diffraction (XRD) measurements. Interestingly, after hydrothermal reduction, a diffraction peak related to rGO

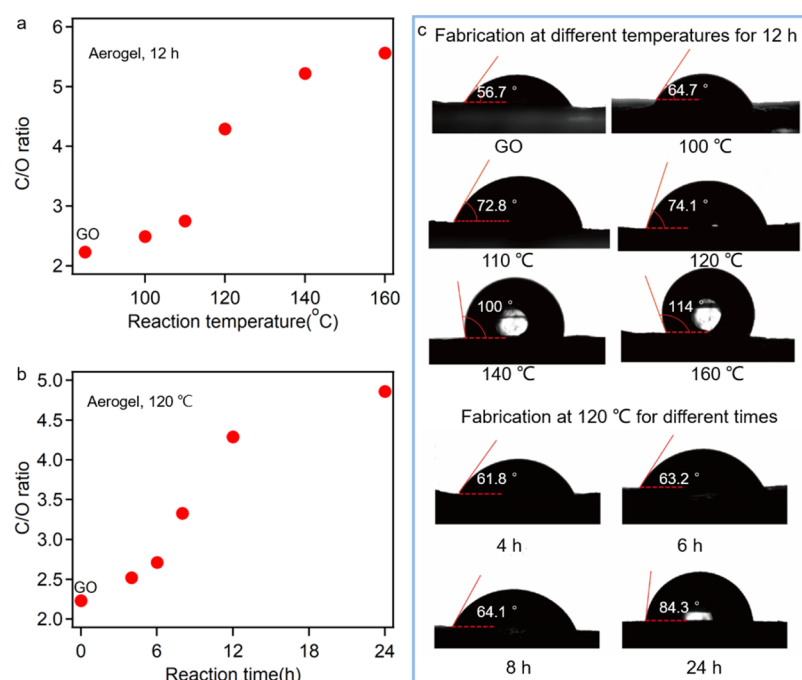


Figure 4. Reduction degree and hydrophilicity of rGO aerogel membranes. (a) Reduction degree of rGO aerogel membranes. (b,c) Hydrophilicity of rGO aerogel membranes.

sheets in the hydrogel appeared at $\sim 27.5^\circ$ (Figure 3b), corresponding to an interlayer distance of ~ 3.3 Å. Besides, the interlayer spacing did not change with temperature or reaction time since 4 h hydrothermal reduction at 120°C (Figure 3b,c), which is close to the theoretical interlayer spacing between adjacent graphene sheets in graphite.³⁴ It means that only a monolayer of water exists in the sub-nanochannels of rGO sheets in the hydrogel. After freeze-drying, the diffraction peak shifts to a lower position at $\sim 22.3^\circ$ (Figure 3d), referring to a sub-nanochannel of ~ 4.0 Å between neighboring rGO sheets in the aerogel membrane. It is a bit larger than the interlayer spacing between rGO sheets in the hydrogel due to the expansion of ice at the frozen state. This agrees with the value of rGO-based aerogels produced by chemical or thermal reduction.^{24,34,48,49} Since the diffraction peak of the rGO laminate in the rGO membrane was broad, which was not different from the sharp diffraction peak of GO¹⁸ and rGO⁴⁵ membranes prepared by vacuum filtration, it means that the graphene sheets were not paralleled perfectly and interlayer spaces between the adjacent graphene sheets varied a bit at around 0.4 nm in the aerogel membrane. Except for the diffraction peak of rGO sheets at 22.3° , a small peak associated to GO structures in the aerogel membranes prepared at 100°C appeared at $\sim 11.6^\circ$ (Figure 3e). This peak disappeared when the temperature was increased above 110°C . When the GO solution was hydrothermally reduced for different times at 120°C , the peak associated to GO laminates shifted to 12.2 and 12.7° , respectively, in 4 h and 6 h, and disappeared after 8 h (Figure 3e). The above results suggest that the GO sheets were not completely reduced into rGO sheets at 100°C and at 120°C in 6 h, which still have similar structural areas to GO sheets.

The graphitization of rGO sheets during the hydrothermal process was studied by Raman measurements (Figure 3f). The D peak of rGO aerogel membranes and GO membranes appeared at the same position of 1346 cm^{-1} , related to the disordered structures of graphene. However, the G peak of

rGO occurred at 1586 cm^{-1} , left-shifted compared to that of GO at 1599 cm^{-1} , which was attributed to the recovery of aromatic structural defects of graphene. The I_D/I_G of rGO aerogel membranes decreased slightly with temperature until 140°C but was much smaller than that of GO membranes, indicating that the defects of graphene structures were repaired during the hydrothermal process.⁴⁹ After 140°C , the temperature has little effects on the further repairing of graphene.

The Fourier-transform infrared spectroscopy (FTIR) spectra of the GO membrane and rGO aerogel membranes were recorded to study the evolution of functional groups with hydrothermal temperature (Supporting Information, Figure S5). The assigned vibration modes of GO have been reported before.^{41,50} The broad band between 2990 and 3610 cm^{-1} is attributed to the O–H stretching vibrations coming from hydroxyl groups in GO and water adsorbed on the GO membrane. The bands at 1033 , 1220 cm^{-1} are due to the vibrations of C–O and –OH groups, respectively. The absorption band at 1615 cm^{-1} is relative to the skeletal vibrations of unoxidized graphitic domains (C=C) or the stretching deformation vibrations of intercalated water, while the band at 1719 cm^{-1} is assigned to the vibrations of C=O groups in carbonyl and carboxyl moieties. The absorption bands of rGO aerogel membranes prepared at 100 and 120°C did not change greatly compared to the GO membrane, meaning that there are still many functional oxygen groups existing in rGO sheets for the aerogel membranes fabricated at a hydrothermal temperature lower than 120°C . For the rGO aerogel membranes synthesized at 140 and 160°C , the bands at 1220 , 1033 , and 1615 cm^{-1} and between 2990 and 3610 cm^{-1} mostly disappeared and the band at 1719 cm^{-1} became weaker, which suggests that the hydroxyl groups were mostly removed at a temperature higher than 140°C , and the band at 1615 cm^{-1} mainly arises from intercalated water and the carboxyl groups were partially removed.

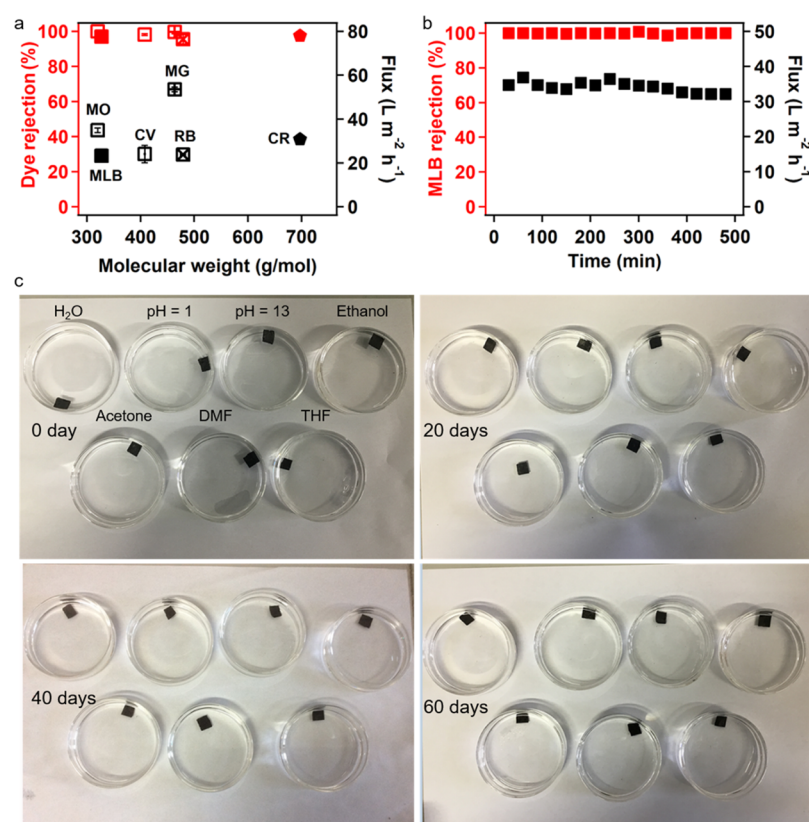


Figure 5. Filtration performance and stability of rGO aerogel membranes. (a) Permeance and rejection of organic dyes (20 mg mL⁻¹) of rGO aerogel membranes. (b) Stability of permeance and rejection of MLB (20 mg mL⁻¹) for rGO aerogel membranes (MLB, MO, CV, MG, RB, and CR). (c) Stability of rGO aerogel membranes in different solvents.

The chemical compositions of the 3D lamellar rGO aerogel membranes and their reduction degrees as a function of hydrothermal temperature and time were studied by X-ray photoelectron spectroscopy (XPS). There are four peaks of C 1s for GO centered at 284.6, 286.7, 287.8, and 288.9 eV, which correspond to C=C/C-C, C-O/C-O-C, C=O, and O=COH groups, respectively⁴¹ (Supporting Information, Figure S6a). Compared to GO, the intensity of the peak at 284.6 eV of rGO aerogel membranes increases with hydrothermal temperature and reaction time, while the peak intensity at 286.7 eV decreases (Supporting Information, Figures S6 and S7), indicating that functional C-OH/C-O-C groups were gradually removed with the increase of temperature. The reduction degrees of rGO aerogel membranes are presented as C/O ratios shown in Figure 4a. The C/O ratio increases slightly with temperature before 110 °C but largely in the range of 110–140 °C and finally slows down after that. When the rGO aerogel membranes were prepared at 120 °C by varying the reaction time, the C/O ratio increased almost linearly with time before 12 h, and after that, it changed slightly (Figure 4b).

The hydrophilicity of rGO aerogel membranes was studied by contact angle measurements (Figure 4c). The contact angle increases from 64.7° for the membrane prepared at 100 °C to 74.1° for the membrane fabricated at 120 °C, which are only a bit higher compared to the one of GO (56.7°), indicating that the aerogel membranes assembled at a temperature lower than 120 °C are still highly hydrophilic. However, once the hydrothermal temperature increases above 140 °C, the membranes become hydrophobic, showing contact angles of

100 and 114° of the rGO aerogel membranes synthesized at 140 and 160 °C, respectively. The contact angle of the rGO membrane prepared at 120 °C increases slightly with reaction time. Even after 24 h of hydrothermal reaction, the contact angle of the membrane is only 84.3°, meaning that the membrane is still hydrophilic. The hydrophilicity benefits the water permeance for the rGO aerogel membranes when used in water purification.⁶

2.3. Water Self-Purification with Dye Aqueous Solutions. Since the GO sheets can be easily self-assembled into a thin hydrogel membrane at 120 °C and its aerogel membrane still maintained the hydrophilicity property, the aerogel membranes fabricated at 120 °C reacting for 12 h were used for water self-purification. To demonstrate the water self-purification property of our aerogel membranes, the permeability and selectivity were analyzed only under the gravity of organic dye aqueous solutions with a 30 cm column height (see the Experimental Section and Supporting Information, Video S3). The dyes used as model compounds include methyl blue (MLB), methyl orange (MO), crystal violet (CV), malachite green (MG), rhodamine B (RB), and congo red (CR) at a concentration of 20 mg L⁻¹. Since the interlayers between adjacent rGO sheets in the laminate are only ~0.4 nm and there are only nanometer and sub-nanometer pores on the surface of the rGO aerogel membrane,⁴⁶ organic dyes could not pass through the membrane, while water molecules could permeate freely through the loose lamellar membrane (see the schematic filtration in Scheme 1). As can be seen from Figure 5a, the rejection of MB, MO, CV, MG, RB, and CR is 99.9% ± 0.1%, 97.0% ± 1.9%, 98.1% ± 0.4%, 99.6% ± 1.0%, 95.6% ±

2.6%, and $97.6\% \pm 1.4\%$, respectively, and the permeance of water ranges from 23 to $53 \text{ L m}^{-2} \text{ h}^{-1}$. The high water flux is ascribed to the loose lamellar structure, in which the laminates were loosely stacked and the laminate consisted of thinner laminates also with large spaces between them.⁴⁶ Similarly, the water flux was increased largely under only water driven of a 10 cm water column by the robust graphene quantum dot-modified thermally reduced graphene oxide membrane, compared to the GO membrane; both were prepared by vacuum filtration. It is because the interlayer spaces between the neighboring graphene sheets were expanded by the graphene quantum dots, and as a result, a high water permeance was obtained only under water driven.⁵⁰ Furthermore, the rGO aerogel membrane shows long stability of water permeance and dye rejection. The rejection of MLB and water permeance did not change for at least 8 h (Figure 5b), which is long enough for portable water purification systems. The overall separation performance of our aerogel membrane is better than that of most nanometer-thick GO-based membranes and can compete with the best ones for selectivities of organic dyes. However, its water permeance has the same magnitude as some of them (Supporting Information, Tables S1 and S2).

In order to exclude the effect of rGO aerogel membranes on the adsorption of organic dyes, we also carried out the filtration measurement of organic dye solutions using porous rGO aerogels prepared at 120°C for 12 h with the bulk hydrothermal reduction method.³⁴ The rGO aerogel with a column height of 5 mm was cut and pressed into a membrane and then used for filtration experiments. Since the aerogel monolith is highly porous, the organic dyes could easily permeate through micrometer pores of the pressed membrane (see the schematic filtration in Scheme 1). As can be seen from Figure S8, even when ~ 4 min filtration was carried out, the porous rGO aerogel cannot effectively adsorb the organic dyes including rejections. The absorption of dyes in the lamellar aerogel membrane was also ruled out by recording the UV-vis spectra of the collected water via filtration of pure water for 1 h, immediately after the filtration of the dye aqueous solution and the mass change of the aerogel membrane by rinsing the top water surface with water and drying the membrane at 60°C for 12 h. After drying the aerogel membrane, the collected didn't have absorption peak or mass change. Thus, it can be concluded that sub-nanochannels and nanochannels, including the narrow interlayer space of adjacent graphene oxide,⁵⁰ and sub-nanometer and nanometer pores on the graphene surface⁴⁶ play a critical role in rejecting the organic compounds.

2.4. Stability of rGO Aerogel Membranes. Since GO membranes are not stable, which can be easily damaged and delaminated in aqueous solutions and some organic solvents,^{6,14,30} we studied the long stability of our 3D lamellar rGO aerogel membranes in aqueous solutions, acid and basic aqueous solutions, and several polar organic solvents. As shown in Figure 5c, the rGO aerogel membranes are stable not only in natural water but also in acidic and basic solutions and several representative polar organic solvents. The rGO aerogel membranes still maintained their original integrity even after 60 days when immersed in the above solvents. It shows that our 3D lamellar rGO aerogel membranes not only have potential in water purification but also might be useful in organic solvents.

3. CONCLUSIONS

In summary, we have successfully fabricated the 3D lamellar rGO hydrogel membranes by a facile, environment-friendly water/vapor interfacial hydrothermal reduction method and their corresponding aerogel membranes with the freeze-drying method. The structures, reduction degrees, chemical compositions, and hydrophilicities of rGO aerogel membranes can be finely tuned by varying the volume of GO dispersions, the hydrothermal temperature, and the reaction time. When used as nanofiltration membranes, the rGO aerogel membranes can effectively reject organic dyes but allow fast water permeation only under the gravity of water. The lamellar rGO aerogel membranes not only are suitable for making cheap, portable water purification devices and home-used water purification systems with no extra power but also have potential in other applications, such as organic solvent separations.

4. EXPERIMENTAL SECTION

4.1. Fabrication of rGO Hydrogel and Aerogel Membranes. Graphene oxide was prepared from natural graphite powder with an average size of $40 \mu\text{m}$ by the modified Hummers method.^{43–45} GO suspensions with a concentration ranging from 1 to 5 mg mL^{-1} were first prepared in water. After that, GO suspension ($0.33\text{--}0.46 \text{ mL cm}^{-2}$, surface concentration) was poured into 10 mL glass vials to synthesize rGO membranes of different size. The 10 mL glass vials were put in 50 mL Teflon containers, and then, all the Teflon containers were put in the corresponding autoclaves. Finally, the autoclaves were put in an oven and heated to the set temperatures ($100, 110, 120, 140,$ and 160°C) from room temperature. After 12 h, there was hydrothermal reaction at each temperature except 120°C , at which the reaction time was varied from 4 to 24 h, and the autoclaves were cooled down to room temperature. As a result, the rGO hydrogels of different sizes were prepared. The rGO aerogel membranes were produced by further freeze-drying the rGO hydrogels after freezing them at $\sim 40^\circ\text{C}$ with a lyophilizer. The porous rGO aerogels were prepared with a similar method as above by pouring $\sim 14 \text{ mL}$ GO suspensions into 25 mL Teflon containers, and the porous rGO aerogel membranes with a 5 mm height were cut from the generated aerogels.

4.2. Characterizations. The GO flake sizes and the morphologies and structures of rGO aerogel membranes were characterized by SEM (Zeiss Ultra 55, Germany). The rGO hydrogel and aerogel membranes were characterized by XRD (Bruker, $\text{Cu K}\alpha$, $\lambda = 0.154 \text{ nm}$, Germany). Raman spectra were recorded using an XploRA spectrometer (Horiba Jobin Yvon, France) with a 532 nm laser source. The chemical compositions of membranes were analyzed by XPS (Thermo Fisher Scientific ESCALAB 250XI, $\text{Al K}\alpha$ source, USA). TGA of rGO hydrogel and aerogel membranes was carried out with a thermal analyzer (Mettler Toledo TGA 1, Swiss) at a heating rate of 10 K min^{-1} under a N_2 atmosphere. Attenuated total reflection-FTIR spectra of rGO aerogel membranes were recorded on a Thermo Fisher Nicolet 6700. Hydrophilicity of the aerogel membranes was evaluated using a contact angle goniometer. UV-vis spectra for the dye solutions were recorded on a Lambda 750 spectrophotometer (PerkinElmer, USA).

4.3. Water Permeability and Dye Rejections of Aerogel Membranes. The rGO aerogel membranes prepared at 120°C for 12 h with a thickness of $\sim 1.2 \text{ mm}$

were used for the study of water permeability and dye rejections. The permeance and dye rejections were measured with an effective membrane area of 2.25 cm² under the gravity of pure water and different dye aqueous solutions of 20 mg L⁻¹ with a homemade column container of a 30 cm height. The pure water permeance of aerogel membranes was analyzed for 30 min first before performing permeance studies using the organic dye aqueous solutions. The filtered water solution was collected for 30 min, and at least a 1 h measurement with the organic dye solution was carried out for each membrane. At least three membranes were used for each dye solution. After the filtration of the dye aqueous solution, pure water was filtered through the membrane for another 1 h. The UV spectra of the collected water were recorded using a UV-vis spectrophotometer. The water flux (J , L m⁻² h⁻¹) and rejection (R , %) were calculated according to eqs 1 and 2, respectively,

$$J = \frac{V}{A\Delta t} \quad (1)$$

$$R = 100 - \frac{C_p}{C_f} \times 100 \quad (2)$$

where V (L) is the volume of permeated water, A (m²) is the effective membrane area, Δt (h) is the permeated time, and C_p and C_f are the concentrations of the permeated and feed solutions, respectively.

After filtration of the dye aqueous solution and pure water, the top membrane surface was rinsed with 5 mL of water, then dried at 60 °C for 12 h, and weighed to check its mass change after the filtration of dye aqueous solutions.

4.4. Stability of Aerogel Membranes. The aerogel membranes prepared at 120 °C for 12 h were cut into small pieces and immersed in pure water, HCl aqueous solution (pH = 1), NaOH aqueous solution (pH = 12), ethanol, acetone, dimethylformamide, and tetrahydrofuran at room temperature. The stabilities of the aerogel membranes were studied after immersion in the abovementioned solutions for 2 months.

■ ASSOCIATED CONTENT

Supporting Information

The Supporting Information is available free of charge at <https://pubs.acs.org/doi/10.1021/acsomega.1c04466>.

Sizes of GO used for preparation of rGO hydrogels and aerogel membranes; cross-section structures and surface morphologies of ~ 0.4 mm thick rGO aerogel membranes prepared at different temperatures for 12 h; cross-section structures of ~ 1.6 mm thick rGO aerogel membranes prepared at 120 °C for 12 h; cross-section structures of ~ 2.0 mm thick rGO aerogel membranes prepared at 120 °C for 12 h; FTIR spectra of GO membranes and rGO aerogel membranes prepared at different temperatures; C 1s spectra of GO membranes and rGO aerogel membranes prepared at different temperatures; C 1s spectra of GO membranes and rGO aerogel membranes prepared at 120 °C for different times; UV spectra of different feed dye solutions and collected solutions filtered with our rGO aerogel membranes prepared by the water/vapor interfacial hydrothermal assembly method and highly porous rGO aerogels prepared with the previous hydrothermal method; separation performance of rGO aerogel membranes for organic dyes; and benchmarks of

graphene-based membranes for organic dye separation (PDF)

Extremely flexible aerogel membrane which can be folded and bent at an extremely low temperature such as in liquid nitrogen with a temperature of -196 °C (MP4)

Extremely flexible aerogel membrane which can be folded and bent at a high temperature of ~100 °C (MP4)

Permeability and selectivity of aerogel membranes analyzed only under the gravity of organic dye aqueous solutions with a 30 cm column height (MP4)

■ AUTHOR INFORMATION

Corresponding Authors

Lili Fu – Zhengzhou Tobacco Research Institute of CNTC, Zhengzhou 450001, China; Guangzhou Institute of Energy Conversion, Chinese Academy of Sciences, Guangzhou 510640, China; orcid.org/0000-0002-4537-0801; Email: lili1101_fu@163.com

Ke Zhang – Zhengzhou Tobacco Research Institute of CNTC, Zhengzhou 450001, China; Email: hfzhangke@126.com

Authors

Pengyu Zhuang – Zhengzhou Tobacco Research Institute of CNTC, Zhengzhou 450001, China; Department of Macromolecular Science, Fudan University, Shanghai 200433, China; orcid.org/0000-0002-0252-6175

Zhongya Guo – Zhengzhou Tobacco Research Institute of CNTC, Zhengzhou 450001, China

Shuang Wang – Zhengzhou Tobacco Research Institute of CNTC, Zhengzhou 450001, China

Qi Zhang – Zhengzhou Tobacco Research Institute of CNTC, Zhengzhou 450001, China; orcid.org/0000-0002-6474-5867

Mingjian Zhang – Zhengzhou Tobacco Research Institute of CNTC, Zhengzhou 450001, China

Han Min – Zhengzhou University, Zhengzhou 450001, China

Bin Li – Zhengzhou Tobacco Research Institute of CNTC, Zhengzhou 450001, China

Complete contact information is available at:

<https://pubs.acs.org/doi/10.1021/acsomega.1c04466>

Notes

The authors declare no competing financial interest.

■ ACKNOWLEDGMENTS

The authors thank Prof. Yuxi Xu at Fudan University for the help.

■ REFERENCES

- (1) Liu, G.; Jin, W.; Xu, N. Graphene-based membranes. *Chem. Soc. Rev.* **2015**, *44*, 5016–5030.
- (2) Park, H. B.; Kamcev, J.; Robeson, L. M.; Elimelech, M.; Freeman, B. D. Maximizing the right stuff: the trade-off between membrane permeability and selectivity. *Science* **2017**, *356*, 1138–1148.
- (3) Peydayesh, M.; Mezzenga, R. Protein nanofibrils for next generation sustainable water purification. *Nat. Commun.* **2021**, *12*, 3248.
- (4) Joshi, R. K.; Carbone, P.; Wang, F. C.; Kravets, V. G.; Su, Y.; Grigorieva, I. V.; Wu, H. A.; Geim, A. K.; Nair, R. R. Precise and ultrafast molecular sieving through graphene oxide membranes. *Science* **2014**, *343*, 752–754.

- (5) Sun, M.; Li, J. Graphene oxide membranes: Functional structures, preparation and environmental applications. *Nano Today* **2018**, *20*, 121–137.
- (6) Thebo, K. H.; Qian, X.; Zhang, Q.; Chen, L.; Cheng, H.-M.; Ren, W. Highly stable graphene-oxide-based membranes with superior permeability. *Nat. Commun.* **2018**, *9*, 1486.
- (7) Bolisetty, S.; Mezzenga, R. Amyloid-carbon hybrid membranes for universal water purification. *Nat. Nanotechnol.* **2016**, *11*, 365–371.
- (8) Ying, Y.; Ying, W.; Li, Q.; Meng, D.; Ren, G.; Yan, R.; Peng, X. Recent advances of nanomaterial-based membrane for water purification. *Appl. Mater. Today* **2017**, *7*, 144–158.
- (9) Cohen-Tanugi, D.; Grossman, J. C. Water desalination across nanoporous graphene. *Nano Lett.* **2012**, *12*, 3602–3608.
- (10) Li, H.; Song, Z.; Zhang, X.; Huang, Y.; Li, S.; Mao, Y.; Ploehn, H. J.; Bao, Y.; Yu, M. Ultrathin, molecular-sieving graphene oxide membranes for selective hydrogen separation. *Science* **2013**, *342*, 95–98.
- (11) Surwade, S. P.; Smirnov, S. N.; Vlassioux, I. V.; Unocic, R. R.; Veith, G. M.; Dai, S.; Mahurin, S. M. Water desalination using nanoporous single-layer graphene. *Nat. Nanotechnol.* **2015**, *10*, 459–464.
- (12) Liu, H.; Wang, H.; Zhang, X. Facile fabrication of freestanding ultrathin reduced graphene oxide membranes for water purification. *Adv. Mater.* **2015**, *27*, 249–254.
- (13) Huang, L.; Chen, J.; Gao, T.; Zhang, M.; Li, Y.; Dai, L.; Qu, L.; Shi, G. Reduced graphene oxide membranes for ultrafast organic solvent nanofiltration. *Adv. Mater.* **2016**, *28*, 8669–8674.
- (14) Morelos-Gomez, A.; Cruz-Silva, R.; Muramatsu, H.; Ortiz-Medina, J.; Araki, T.; Fukuyo, T.; Tejima, S.; Takeuchi, K.; Hayashi, T.; Terrones, M.; Endo, M. Effective NaCl and dye rejection of hybrid graphene oxide/graphene layered membranes. *Nat. Nanotechnol.* **2017**, *12*, 1083–1088.
- (15) Wang, L.; Boutillier, M. S. H.; Kidambi, P. R.; Jang, D.; Hadjiconstantinou, N. G.; Karnik, R. Fundamental transport mechanisms, fabrication and potential applications of nanoporous atomically thin membranes. *Nat. Nanotechnol.* **2017**, *12*, 509–522.
- (16) Prozorovska, L.; Kidambi, P. R. State-of-the-art and future prospects for atomically thin membranes from 2D Materials. *Adv. Mater.* **2018**, *30*, 1801179.
- (17) Huang, H.; Ying, Y.; Peng, X. Graphene oxide nanosheet: an emerging star material for novel separation membranes. *J. Mater. Chem. A* **2014**, *2*, 13772.
- (18) Nair, R. R.; Wu, H. A.; Jayaram, P. N.; Grigorieva, I. V.; Geim, A. K. Unimpeded permeation of water through Helium-Leak-Tight graphene-based membranes. *Science* **2012**, *335*, 442–444.
- (19) Mao, L.; Park, H.; Soler-Crespo, R. A.; Espinosa, H. D.; Han, T. H.; Nguyen, S. T.; Huang, J. Stiffening of graphene oxide films by soft porous sheets. *Nat. Commun.* **2019**, *10*, 3677.
- (20) Mouhat, F.; Coudert, F.-X.; Bocquet, M.-L. Structure and chemistry of graphene oxide in liquid water from first principles. *Nat. Commun.* **2020**, *11*, 1566.
- (21) Paul, D. R. Creating new types of carbon-based membranes. *Science* **2012**, *335*, 413–414.
- (22) Koenig, S. P.; Wang, L.; Pellegrino, J.; Bunch, J. S. Selective molecular sieving through porous graphene. *Nat. Nanotechnol.* **2012**, *7*, 728–732.
- (23) Celebi, K.; Buchheim, J.; Wyss, R. M.; Droudian, A.; Gasser, P.; Shorubalko, I.; Kye, J.-I.; Lee, C.; Park, H. G. Ultimate permeation across atomically thin porous graphene. *Science* **2014**, *344*, 289–292.
- (24) Su, Y.; Kravets, V. G.; Wong, S. L.; Waters, J.; Geim, A. K.; Nair, R. R. Impermeable barrier films and protective coatings based on reduced graphene oxide. *Nat. Commun.* **2014**, *5*, 4843.
- (25) Dreyer, D. R.; Park, S.; Bielawski, C. W.; Ruoff, R. S. The chemistry of graphene oxide. *Chem. Soc. Rev.* **2010**, *39*, 228–240.
- (26) Abraham, J.; Vasu, K. S.; Williams, C. D.; Gopinadhan, K.; Su, Y.; Cherian, C. T.; Dix, J.; Prestat, E.; Haigh, S. J.; Grigorieva, I. V.; Carbone, P.; Geim, A. K.; Nair, R. R. Tunable sieving of ions using graphene oxide membranes. *Nat. Nanotechnol.* **2017**, *12*, 546–550.
- (27) Chen, L.; Shi, G.; Shen, J.; Peng, B.; Zhang, B.; Wang, Y.; Bian, F.; Wang, J.; Li, D.; Qian, Z.; Xu, G.; Liu, G.; Zeng, J.; Zhang, L.; Yang, Y.; Zhou, G.; Wu, M.; Jin, W.; Li, J.; Fang, H. Ion sieving in graphene oxide membranes via cationic control of interlayer spacing. *Nature* **2017**, *550*, 380–383.
- (28) Dikin, D. A.; Stankovich, S.; Zimney, E. J.; Piner, R. D.; Dommett, G. H. B.; Evmenenko, G.; Nguyen, S. T.; Ruoff, R. S. Preparation and Characterization of Graphene Oxide Paper. *Nature* **2007**, *448*, 457–460.
- (29) Yang, Q.; Su, Y.; Chi, C.; Cherian, C. T.; Huang, K.; Kravets, V. G.; Wang, F. C.; Zhang, J. C.; Pratt, A.; Grigorenko, A. N.; Guinea, F.; Geim, A. K.; Nair, R. R. Ultrathin graphene-based membrane with precise molecular sieving and ultrafast solvent permeation. *Nat. Mater.* **2017**, *16*, 1198–1202.
- (30) Ying, Y.; Ying, W.; Guo, Y.; Peng, X. Cross-flow-assembled ultrathin and robust graphene oxide membranes for efficient molecule separation. *Nanotechnology* **2018**, *29*, 155602.
- (31) Yeh, C.-N.; Raidongia, K.; Shao, J.; Yang, Q. H.; Huang, J. On the origin of the stability of graphene oxide membranes in water. *Nat. Chem.* **2015**, *7*, 166–170.
- (32) Li, D.; Müller, M. B.; Gilje, S.; Kaner, R. B.; Wallace, G. G. Processable Aqueous Dispersions of Graphene Nanosheets. *Nat. Nanotechnol.* **2008**, *3*, 101–105.
- (33) Han, Y.; Xu, Z.; Gao, C. Ultrathin graphene nanofiltration membrane for water purification. *Adv. Funct. Mater.* **2013**, *23*, 3693–3700.
- (34) Xu, Y.; Sheng, K.; Li, C.; Shi, G. Self-assembled graphene hydrogel via a one-step hydrothermal process. *ACS Nano* **2010**, *4*, 4324–4330.
- (35) Qiu, L.; Liu, J. Z.; Chang, S. L. Y.; Wu, Y.; Li, D. Biomimetic superelastic graphene-based cellular monoliths. *Nat. Commun.* **2012**, *3*, 1241.
- (36) Lv, W.; Zhang, C.; Li, Z.; Yang, Q.-H. Self-assembled 3D graphene monolith from solution. *J. Phys. Chem. Lett.* **2015**, *6*, 658–668.
- (37) Hu, K.; Xie, X.; Szkopek, T.; Cerruti, M. Understanding hydrothermally reduced graphene oxide hydrogels: from reaction products to hydrogel properties. *Chem. Mater.* **2016**, *28*, 1756–1768.
- (38) Xu, Y.; Lin, Z.; Zhong, X.; Papandrea, B.; Huang, Y.; Duan, X. Solvated graphene frameworks as high-performance anodes for lithium-ion batteries. *Angew. Chem., Int. Ed.* **2015**, *54*, 5345–5350.
- (39) Xu, Y.; Lin, Z.; Huang, X.; Wang, Y.; Huang, Y.; Duan, X. Functionalized graphene hydrogel-based high-performance supercapacitors. *Adv. Mater.* **2013**, *25*, 5779–5784.
- (40) Cong, H.-P.; Ren, X.-C.; Wang, P.; Yu, S.-H. Macroscopic multifunctional graphene-based hydrogels and aerogels by a metal ion induced self-assembly process. *ACS Nano* **2012**, *6*, 2693–2703.
- (41) Tiwari, J. N.; Mahesh, K.; Le, N. H.; Kemp, K. C.; Timilsina, R.; Tiwari, R. N.; Kim, K. S. Reduced graphene oxide-based hydrogels for the efficient capture of dye pollutants from aqueous solutions. *Carbon* **2013**, *56*, 173–182.
- (42) Lim, H. N.; Huang, N. M.; Lim, S.; Harrison, I.; Chia, C. Fabrication and characterization of graphene hydrogel via hydrothermal approach as a scaffold for preliminary study of cell growth. *Int. J. Nanomed.* **2011**, *6*, 1817–1823.
- (43) Hummers, W. S.; Offeman, R. E. Preparation of graphitic oxide. *J. Am. Chem. Soc.* **1958**, *80*, 1339.
- (44) Xu, Y.; Bai, H.; Lu, G.; Li, C.; Shi, G. Flexible graphene films via the filtration of water-soluble noncovalent functionalized graphene sheets. *J. Am. Chem. Soc.* **2008**, *130*, 5856–5857.
- (45) Xu, Z.; Gao, C. Aqueous liquid crystals of graphene oxide. *ACS Nano* **2011**, *5*, 2908–2915.
- (46) Zhuang, P.; Fu, H.; Xu, N.; Li, B.; Xu, J.; Zhou, L. Free-standing reduced graphene oxide (rGO) membrane for salt-rejecting solar desalination via size effect. *Nanophotonics* **2020**, *9*, 4601–4608.
- (47) Wan, W.; Zhang, F.; Yu, S.; Zhang, R.; Zhou, Y. Hydrothermal formation of graphene aerogel for oil sorption: the role of reducing agent, reaction time and temperature. *New J. Chem.* **2016**, *40*, 3040–3046.

(48) Moon, I. K.; Lee, J.; Ruoff, R. S.; Lee, H. Reduced graphene oxide by chemical graphitization. *Nat. Commun.* **2010**, *1*, 73.

(49) Qin, Y.; Peng, Q.; Ding, Y.; Lin, Z.; Wang, C.; Li, Y.; Xu, F.; Li, J.; Yuan, Y.; He, X.; Li, Y. Lightweight, superelastic, and mechanically flexible graphene/polyimide nanocomposite foam for strain sensor application. *ACS Nano* **2015**, *9*, 8933.

(50) Ying, Y.; He, P.; Wei, M.; Ding, G.; Peng, X. Robust GQDs Modified Thermally Reduced Graphene Oxide Membranes for Ultrafast and Long-Term Purification of Dye-Wasted Water. *Adv. Mater. Interfaces* **2017**, *4*, 1700209.